NASA
Technical
Paper
2736

August 1987

Steady and Unsteady Aerodynamic Forces From the SOUSSA Surface-Panel Method for a Fighter Wing With Tip Missile and Comparison With Experiment and PANAIR

Herbert J. Cunningham

NASA

NASA Technical Paper 2736

1987

Steady and Unsteady Aerodynamic Forces From the SOUSSA Surface-Panel Method for a Fighter Wing With Tip Missile and Comparison With Experiment and PANAIR

Herbert J. Cunningham

Langley Research Center
Hampton, Virginia

National Aeronautics and Space Administration

Scientific and Technical Information Office

Summary

The SOUSSA surface-panel computer program for calculating aerodynamic forces for potential flow was applied to a thin fighter-type wing model with and without a tip-mounted missile. Steady and unsteady lift and pitching-moment results are presented for the Mach number M range 0.6 to 0.9 and are compared with results from experiments and from PANAIR and related computer programs. In general, the SOUSSA program, the experiments, and the three PANAIR (and related) programs give lift and pitching-moment results which agree at least fairly well, except for the unsteady experimental moment at $M = 0.8$ for the clean wing and the unsteady moment at $M = 0.8$ calculated with a PANAIR-predecessor program for the wing with tip-mounted missile.

Introduction

There has been a continuing quest for more (and more detailed) accuracy in determining both steady and unsteady aerodynamic forces on wings and bodies in the various Mach number ranges. Integral-equation methods have been developed which account for the actual body shape, thickness, and position (orientation) without resorting to in-plane or on-axis approximations. A leading approach is to evaluate the required integrals by subdividing the surface into an array of connected panels, prescribing a functional form for the variation of the dependent variable (e.g., velocity potential) over each panel, and calculating the effect of each panel on all panels. A number of such panel methods exist which apply to steady flow over a motionless body.

In contrast, for unsteady motions there are few calculation methods available, despite the fact that the unsteady capability is of growing importance for aeroelastic behavior, control motions, gusts, and other transient considerations. The present report concerns applications and validation of a calculation method which does account for unsteady motions and deformations. For inviscid isentropic flow, Morino (1974, 1980) employed a generalized Green's function method which transforms the full velocity-potential differential equation into an integral-differential delay equation whose solution for linearized subsonic flow is implemented in the prototype computer program SOUSSA P1.1 (Morino 1980 and Smolka et al. 1980). This program employs a velocity potential that is spatially constant over each panel, and it is thus termed a "zero-order" method.

An earlier validation and critique of SOUSSA P1.1 was provided by Yates et al. (1982) for five simple wing planforms and for one wing-with-fuselage configuration. The purpose of the present report is to extend the validation to a more geometrically complex and more realistic configuration, that of the instrumented F-5 fighter wing model both without and with a tip-mounted launcher and missile, for which the experimental results appear in the reports by Tijdeman et al. (1978, 1979). Effects of panel arrangement and density are studied.

In order to provide comparisons with other panel methods, calculated results from two PANAIR programs and from a predecessor of PANAIR are also presented. A PANAIR program in use at the Langley Research Center (see Derbyshire and Sidwell 1982) has the capability to calculate only steady forces and was used in calculations for the clean wing; these results are denoted by PANAIR(S). Another PANAIR program, a pilot code (see Dusto and Epton 1980), was used to calculate both steady and unsteady comparative results for the clean wing; these results are denoted by PANAIR(U). From a higher-order-panel method program (predecessor of PANAIR; see Dusto 1980), steady and unsteady results are included for comparison of both the clean wing and the wing plus tip-mounted launcher and missile body. These three programs solve the linear integral equation of unsteady or steady small-disturbance subsonic potential flow. The wing-body surface is divided into panel, and the surface boundary conditions are imposed on the actual steady mean panel locations. On each panel the velocity potential is approximated by linearly distributed sources and quadratically distributed doublets; hence, the term "higher-order method" is used. The strengths of sources and doublets are solved by satisfying the boundary conditions. Calculations were made in the Mach number range of 0.6 to 0.9. Results are presented in figures and listed in tables.

Symbols

Subscript Z appears in Tijdeman et al. (1978, 1979) to identify normal force, which differs only insignificantly from lift force in this investigation.

$C_{L_\alpha}, C^*_{Z_\alpha}$	lift-curve slope, per radian
C_M	pitching-moment coefficient about root midchord axis
C^*_M	tip-body contribution to pitching-moment coefficient about axis at strain-gage "balance center" (i.e., 75.0-percent root chord)
$C_{M_\alpha}, C^*_{M_\alpha}$	pitching-moment-curve slope about root midchord axis, per radian

C_P	pressure coefficient
C_Z	lift coefficient
C_Z^*	tip-body contribution to lift coefficient
c	local chord, in.
Im( )	imaginary part of ( )
i	imaginary number
M	free-stream Mach number
Re( )	real part of ( )
x	local streamwise coordinate, in.
α	angle of attack, deg
η	spanwise coordinate normalized to semispan

Analysis

The SOUSSA Program

For small perturbations and subsonic Mach numbers, the integral equation (2-52) of Morino (1980) expresses the relationship between the perturbation velocity potential Φ and downwash Ψ at the surface of the body as follows (in the symbols of that report):

$$4\pi E(\overline{P}_*)\Phi(\overline{P}_*,T_*) = -\iint_{\Sigma_B}[\Psi]^\theta \frac{1}{R}\,d\Sigma_B + \iint_{\Sigma_B}\left([\Phi]^\theta \frac{\partial}{\partial N}\left[\frac{1}{R}\right] - \left[\frac{\partial\Phi}{\partial T}\right]^\theta \frac{1}{R}\frac{\partial\theta}{\partial N}\right)d\Sigma_B + \iint_{\Sigma_W}\left([\Delta\Phi]^\theta \frac{\partial}{\partial N_u}\left(\frac{1}{R}\right) - \left[\frac{\partial\Delta\Phi}{\partial T}\right]^\theta \frac{1}{R}\frac{\partial\hat{\theta}}{\partial N_u}\right)d\Sigma_W$$

The velocity potential at body surface point P_* at present time T_* is given on the left-hand side of the equation. On the right-hand side are all the effects from perturbations that originated in past time T from the body and wake surfaces, Σ_B and Σ_W respectively. The quantity R is the Prandtl-Glauert transformed distance traveled by a perturbation in reaching P_*. The first integral represents a distribution of sources, the strength of which is the local value of downwash on the body surface. The second integral represents the effect from a distribution of doublets which arise from the interrelation of velocity potentials on the body surface, and the third integral represents the effect from "wakelets," the doublets distributed on the wake.

The body surface Σ_B is discretized by quadrilateral panels with hyperboloidal surfaces. The velocity potential on each panel is assumed to be spatially constant and of unknown complex amplitude. The values of these complex amplitudes are obtained from the solution of the set of simultaneous equations, one for each panel. The program originally provided for a finite-panel wake of arbitrary shape, but it was much more economical and satisfactory in the present usage to analyze the wake as flat and extending downstream to infinity in strips from the trailing edge, subject to the Kutta condition, and with properties sinusoidally varying downstream according to the past history of harmonic motion. An addendum to the SOUSSA manual by Cunningham, Desmarais, and Yates (1982) describes the added data which control the wake treatment used herein.

The most general configuration to which any version of SOUSSA has been applied is the Space Shuttle. The full-span vehicle was divided into 764 panels. Symmetric and antisymmetric subsonic flutter analyses were made with 60 vibration modes, including control-surface modes. Also the external tank and solid-rocket boosters were modeled and the calculations were obtained for the launch configuration. This unpublished work was described by Yates (1986).

A variety of more recent experiences, as well as a critique of the program, is given by Yates et al. (1982). Five different wing configurations and one wing-body configuration were analyzed, and steady and unsteady pressure distributions, generalized aerodynamic forces, and flutter-boundary calculations were presented. The resulting comparisons with experimental results and other analyses were mostly very good.

PANAIR and Predecessor Programs

The fundamental integral equation for the linear steady perturbation velocity potential of PANAIR was obtained by applying Green's third identity to convert Laplace's equation, and it appears as equation (3.2.7) of Magnus and Epton (1980), namely

$$\phi(P) = -\frac{1}{4\pi}\iint_S\left[\frac{\sigma}{R} - \mu\hat{n}\cdot\nabla\left(\frac{1}{R}\right)\right]dS$$

where $\phi(P)$ is the perturbation velocity potential at point P on the surface S of the body plus the wake. At arbitrary integration points on S, R is

the "compressible" distance to P, $\hat{n}$ is the unit normal, σ and μ are the unknown source and doublet strengths, respectively, and ∇ is the gradient operator. On the other hand, for the PANAIR-predecessor higher-order-panel method used by Dusto (1980), the integral equation derives from the application of the Prandtl-Glauert transformation to Helmholtz's equation for the unsteady potential function. From pages 3 and 4 of Dusto and Epton (1980) the integral equation is (sic)

$$\phi^*(P) = \frac{1}{4\pi} \iint_S \left\{ \sigma^*(Q) \frac{e^{-i\Omega R}}{R} - \mu^*(Q) \frac{\partial}{\partial n} \left(\frac{e^{-i\Omega R}}{R} \right) \right\} dS$$

where Q is the surface integration point, $\Omega = \omega/(a\beta^2)$ where ω is circular frequency, a is speed of sound, and $\beta^2 = (1-M^2)$, σ^* and μ^* are the complex amplitudes of source and doublet strengths, respectively, and S, R, and $\hat{n}$, have the same meanings as in the preceding equation. The close parallelism of the two integral equations above is apparent. The difference in signs comes from the chosen positive senses of the unit normal $\hat{n}$. There also exists a PANAIR pilot code that includes the unsteady oscillation effects, and with this code a few results were calculated for comparison.

The body surface (and optionally the wake) is divided into panels, and over each panel there is permitted a linear variation of source strength and a quadratic variation of doublet strength. For each point P the surface integrations are subdivided into the contributions from each panel per unit value of the strengths. The result is a set of simultaneous equations whose left-hand side consists of a matrix of velocity-potential influence coefficients times a column vector of unknown source and doublet strengths. The right-hand side of the equation set implements the boundary and the Kutta conditions.

Configuration Definition

For the present analysis the configuration studied is the F-5 fighter wing model for which experimental results are reported in the reports by Tijdeman et al. (1978, 1979). The half-span wing (see fig. 1) has a leading-edge sweep of 31° 55′, a taper ratio of 0.308, a full-span aspect ratio of 2.98, and a 4.8-percent-thick airfoil. The airfoil section has a slight nose-down camber over the forward 40 percent of the chord but is symmetric over the aft 60 percent. The clean wing was tested with a rounded tip fairing. For the tests with tip-mounted body the tip fairing was replaced with a long, slender missile launcher, and the missile body was mounted against the launcher with no gap.

The clean wing, including the tip fairing, is sketched in figure 1. Figure 2 diagrams the wing with missile launcher and missile body. Also shown in figure 2 is the panelling of the wing and the tip body as analyzed with the higher order panelling method and reported in Dusto (1980). This panelling is based on a nearly cosine distribution plus certain additional subdivisions and is termed the "13 × 13 cosine modified" panelling. (See tables 1 and 2 of Dusto 1980.) Figure 3 shows perspective views of the wing with tip body panelled for SOUSSA analysis. All 634 panels, including the far-side ones, are shown. The wing itself is divided into panels with a 10×10 unform distribution. Figure 3(a) is an overall view, and figure 3(b) is a close-up of the tip body. The body panelling at the tip juncture had to be the same streamwise, and the rest of the tip body was divided into panels with about the same fineness, which was thought to be adequate. In general, the 434 tip-body panels were approximately square.

Results and Discussion

The SOUSSA results were calculated mainly for comparison with the available experimental data at subsonic Mach numbers of 0.6 and 0.8 and extending to $M = 0.9$ for the wing with the tip body, for which $M = 0.8$ was not tested. Other available panel-method results from PANAIR and PANAIR-related programs are included for comparison. Dusto's (1980) results for the clean wing at $M = 0.6$ and 0.8 and for the wing with tip body at $M = 0.8$ are included. Also, as stated in the *Introduction*, a few other calculations, designated PANAIR(S) and PANAIR(U), are presented for the clean wing. The results are organized as indicated in the table on page 4. All figures except 7(b) include experimental results. All experimental and calculated data presented in the figures are also tabulated. Table I for the clean wing and table II for the wing with tip body list lift and moment and their slopes with respect to angle of attack.

Results are given for the clean wing with tip fairing in figures 4 and 5 for $M = 0.6$ and 0.8, and for the wing plus tip-mounted launcher and missile body (no fins) in figures 6 and 7 for $M = 0.6$, 0.8, and 0.9. The steady lift and moment coefficients are given for $\alpha = -0.5°$, 0°, 0.5°. The unsteady results are the complex amplitudes of lift- and moment-curve slopes (per radian) for small-amplitude (±0.11° for clean wing, ±0.52° with tip body) pitching oscillations about the root midchord axis. For the wing with tip body, the lift and moment results are given for the entire configuration and separately for the tip body itself. The experimental results were obtained

on the wing by chordwise integration of pressures for the section values and then by spanwise integration of the section values for total results. The tip-body contributions are from strain-gage data.

Figure	Method	Panelling	Variable (a)	Motion
Clean wing				
4(a)	SOUSSA	10 × 10, uniform	P	Steady
4(a)	SOUSSA	12 × 12, uniform	P	Steady
4(a), 4(b)	SOUSSA	13 × 13, cosine, modified	P	Steady
4(a), 4(b)	Dusto	13 × 13, cosine, modified	M	Steady
4(a)	PANAIR(S)	13 × 13, cosine, modified	M	Steady
4(a)	PANAIR(S)	10 × 10, uniform	P	Steady
4(b)	PANAIR(U)	13 × 13, cosine, modified	P	Steady
4(b)	SOUSSA	13 × 13, uniform	P, M	Steady
5(a)	SOUSSA	10 × 10, uniform	P, M	Steady
5(a)	SOUSSA	13 × 13, cosine, modified	P	Unsteady
5(a), 5(b)	Dusto	13 × 13, cosine, modified	P	Unsteady
5(a)	PANAIR(S)	13 × 13, cosine, modified	M	Unsteady
5(b)	SOUSSA	13 × 13, uniform	M	Steady
5(b)	PANAIR(U)	13 × 13, cosine, modified	M	Unsteady
				Unsteady
Wing with tip body				
6(a), 6(b)	SOUSSA	10 × 10, uniform (wing)		Steady
7(a)–7(c)	SOUSSA	10 × 10, uniform (wing)		Unsteady
7(b)	Dusto	13 × 13, cosine, modified		Unsteady

[a]P—Panelling; M—Method.

Clean Wing

Steady. Figures 4(a) for $M = 0.6$ and 4(b) for $M = 0.8$ show steady lift coefficient C_Z and pitching-moment coefficient C_M (about root mid-chord axis) for $\alpha = -0.5°$, 0°, and 0.5°. Here and for other steady results the sloping lines connect selected points for the three angles of attack. The experimental values (square symbols) are from test runs 136, 137, and 138 ($M = 0.6$) and runs 145, 146, and 147 ($M = 0.8$) of Tijdeman et al. (1978, 1979). It is not known why the experimental values vary nonlinearly at these small angles of attack. The nonlinearity may be caused by the combination of forward camber and the relatively sharp leading edge, which results in sizeable down loads over the foremost part of the wing, even at $\alpha = 0.5°$. (See fig. 4(c) discussion below.) For $M = 0.6$ (fig. 4(a)), there are SOUSSA results for three different wing panellings: 10 × 10 uniform (i.e., 10 chordwise and 10 spanwise), 12 × 12 uniform, and 13 × 13 cosine modified. The latter panelling is that employed in Dusto (1980) (as illustrated in his fig. 18 for clean wing with tip fairing) and is used for comparison. These three SOUSSA results are closely bunched together, thereby indicating a substantial convergence with respect to the panelling. The SOUSSA lift and moment coefficients are shown to be a little higher than the experimental values (except for $\alpha = -0.5°$), with the slopes of the lift curves being about the same and the slope of the SOUSSA moment curves being a little higher than the experimental moment curve. Dusto's results are given by the open circles, and both the lifts and the moments are slightly above the SOUSSA results. It is not known why the DUSTO lift at $\alpha = 0°$ is not negative. The steady PANAIR program was applied for the same 13 × 13 panelling used by Dusto. The resulting values (open diamond symbols, designated PANAIR(S)) fall among the SOUSSA results. However, the PANAIR(S) code with the 10 × 10 uniform panelling results in both lift and moment coefficients which are sharply different from the other results. This difference is unexpected and is thought to be caused by the relatively large leading-edge panels and the associated calculation of lifting pressure behind the leading-edge peak.

Figure 4(b) compares calculations from three different codes with experimental values for $M = 0.8$. The Dusto (1980) results with the 13×13 cosine modified panelling and the SOUSSA results with the 13×13 uniform panelling have the same relative positions as for $M = 0.6$; that is, the analytical results are moderately above the experimental values, except at $\alpha = 0.5°$, and the Dusto results are near and above the SOUSSA results. The unsteady PANAIR(U) pilot code results are given by the solid circles. They are very close to the SOUSSA lift results but are distinctly below the experimental moment results. All the calculations overpredicted C_Z at $\alpha = 0°$ and its slope C_{L_α} somewhat, as is typical for potential flow methods.

Figure 4(c) gives a comparison of SOUSSA and experimental pressure distributions at three span stations for $M = 0.8$ and $\alpha = 0.5°$. The SOUSSA results from a 13×13 uniform panelling are plotted as straight-line segments connecting the panel-center values. At the inboard and midspan stations, SOUSSA pressures are mostly below the experimental values over the forward part of the chord, although lifting pressure differences are well predicted. Outboard, however, forward lifting pressure are slightly underpredicted. As mentioned previously, both calculation and experiment indicate sizeable down loads on the foremost part of the wing all across the span, even for $\alpha = 0.5°$.

Unsteady. Figures 5(a) for $M = 0.6$ and 5(b) for $M = 0.8$ show the slopes (per radian) of the complex amplitude of the lift coefficient and of the pitching-moment coefficient for small amplitude ($\pm 0.11°$) pitching oscillations about the zero mean angle of attack. In part II of their report, Tijdeman et al. (1979) list the oscillation amplitude as 0.11°. For both Mach numbers, in addition to the quasisteady values there are experimental values for two pitching frequencies, 20 and 40 Hz, a Dusto (1980) result for 40 Hz, and SOUSSA results for 0, 20, and 40 Hz. Here and for other unsteady results the lines from the origin to selected points serve to display the phase angle of that complex result. The reduced frequency for 40 Hz is 0.399 for $M = 0.6$ and is 0.307 for $M = 0.8$, based on root half-chord. Each calculation used the matching experimental reduced frequencies. The quasisteady results are inferred from the slope of the static results. For $M = 0.8$, the PANAIR(U) results also are presented.

For $M = 0.6$ (fig. 5(a)), the calculated and experimental results display fair to good agreement. In comparison to experimental results, calculated lift and moment magnitudes are about 25 percent larger, moment phase angles agree well, SOUSSA lift phase angles are a few percent less (about 5°) for 20 Hz but are 20 to 30 percent less at 40 Hz, and the Dusto (1980) lift phase angle is about 45 percent (about 12°) less at 40 Hz. The agreement between the SOUSSA results and the experimental results improves significantly as the panelling is made finer, thereby indicating that the convergence with respect to panelling is not as well established for the unsteady case as for the steady case.

Figure 5(b) gives the calculated and experimental results for $M = 0.8$. Compared with the experimental lift-slope magnitudes, SOUSSA magnitudes are about 30 percent larger, PANAIR(U) magnitudes are about 25 percent larger, and Dusto (1980) magnitudes are 35 to 45 percent larger. All the calculated lift-slope phase angles are smaller than the experimental angles—the SOUSSA by 40 percent (about 9° at 40 Hz), the PANAIR(U) by 55 percent (about 12°), and the Dusto (1980) by 65 percent (about 15° at 40 Hz). For the moment slope the experimental quasisteady moment slope is positive (i.e., in the pitch-divergent sense) as for all other cases studied, but for 20 and 40 Hz the moment slope has shifted over into the third quadrant, indicating a real part that opposes pitch displacement. This shift from the 0-Hz to the 20-Hz moment slope represents a rearward shift of center of lift by 8 percent of root chord. The negative imaginary part continues to damp the pitching velocity.

In contrast to the experimental results, all the calculated moment slopes are in the fourth quadrant. For all frequencies the SOUSSA moment magnitudes are twice the experimental values, and the PANAIR(U) magnitudes are even higher. In comparison with SOUSSA, the Dusto (1980) result for 40 Hz is very close. It is notable and somewhat surprising that the PANAIR(U) code, with its higher order panels, has not given a plainly better result than the SOUSSA code with its "zero order" (i.e., constant potential) panels. Here again, as in figures 4(a) and 4(b), all the calculations substantially overpredict the magnitudes of both C_{L_α} and C_{M_α} at both Mach numbers.

Figure 5(c) shows distributions of lifting-pressure slope results from SOUSSA and experiment at three span stations at $M = 0.8$ for pitching motion about $\alpha = 0°$. The real and imaginary parts of the complex amplitude (per radian) are plotted. The SOUSSA results are plotted as straight-line segments connecting the 13 panel-center values. The chordwise distribution of experimental lifting-pressure slopes show a strong reversal at the most forward data point for $\eta = 0.18$, a less strong reversal for $\eta = 0.51$, and no reversal for $\eta = 0.87$. The SOUSSA results show no reversals with the relatively coarse panelling

used near the leading edge. Aft of the most forward data point the SOUSSA results agree well for the imaginary part and somewhat less well for the real part, with some underprediction of the real part for $x/c = 0.20$ to 0.40, and some over prediction aft for $x/c = 0.70$ to 0.90.

Wing With Tip Body

The remaining results are for the wing plus tip-mounted launcher and missile body. For such a geometrically complex configuration the SOUSSA program requires a large amount of tightly organized and coordinated geometrical input data, which is generated by a preprocessor program. The preprocessor program used was not efficiently organized, and as a result only a limited number of panels could be generated within the available machine core memory (131 072 words in a CDC 6600 computer). Because of this preprocessor limit, the wing plus tip body was divided into 634 panels, with the wing upper and lower surfaces each containing 10 panels chordwise by 10 spanwise. Relatively few additional panels could have been accommodated, and hence the fins could not be added.

In each figure the total configuration results appear at the left, and the contributions from the tip body appear at the right. The reference wing area is the clean-wing area for all coefficients. The moment reference length is the mean geometric chord, 0.4183 m. The tip-body pitching moment C_M^* is referenced about an axis at the strain-gage balance center at 75.0 percent of the root chord.

Steady. The steady results are given in figures 6(a) for $M = 0.6$ and 6(b) for $M = 0.9$. The comparison between the experimental and the SOUSSA results is good. In fact, the comparison is mostly better than for the clean wing in figure 4. The agreement for the tip-body contributions is especially good. For $M = 0.6$, the SOUSSA lift magnitudes at $\alpha = \pm 0.5°$ and the lift-curve slope are increased by about 10 percent over that of the clean wing, while the lift on the tip body is just under 3 percent of the total. This indicates a significant "end plate" effect of the tip body acting on the wing. The upsetting moment is decreased by nearly 10 percent because the increased lift is added largely behind the pitch axis, and it contributes in the restoring sense (i.e., negatively). For $M = 0.9$ the comparisons are very similar to those for $M = 0.6$.

Unsteady. Figures 7(a) for $M = 0.6$, 7(b) for $M = 0.8$, and 7(c) for $M = 0.9$ show the unsteady results for the total configuration on the left and the tip-body contributions on the right. For $M = 0.6$, the magnitudes of the total-configuration lift-curve slopes from SOUSSA for all three frequencies are about 10 percent greater than for the clean wing of figure 5(a). The tip-body contributes less than 3 percent of this lift, thereby again indicating an end-plate effect of the tip body. This increased lift near the tip acts to resist the pitch displacement and causes the SOUSSA total-configuration moment-curve slope to be about 10 percent less than for the clean wing. The magnitudes of the SOUSSA total-configuration lift curve, total-configuration moment curve, and tip-body moment curve are about 25 percent greater than the 20-Hz experimental values, and the SOUSSA tip-body lift curve is slightly less than the experimental.

For $M = 0.8$ (fig. 7(b)), there are no experimental results but there are comparisons of the quasi-steady and 40-Hz results from SOUSSA and Dusto (1980). The comparisons are fairly good except for the pitching moment. The Dusto (1980) pitching-moment slope in the third quadrant is from his table 9 for configuration C4. The reason for the different quadrant is not known, although Dusto states that the Kutta condition was not achieved in the unsteady case, thereby implying that an improvement was needed. For the other three comparisons, the SOUSSA phase is consistently greater by a considerable percentage margin, although all the phase angles are rather small.

For $M = 0.9$ (fig. 7(c)), there are comparisons of the quasisteady and the 20-Hz SOUSSA and experimental results. At 20 Hz the reduced frequency is 0.138 (reference length is the root half-chord). The pitch amplitude of the experiment is 0.53°. The SOUSSA lift-curve and moment-curve magnitudes are somewhat greater than experimental magnitudes for the total configuration but are somewhat less for the tip-body contribution. For all results except the total-configuration moment curve, the SOUSSA phase angle is about double that of the experiment, although again all phase angles are small. For the total-configuration moment curve, the phase angle agreement is good. Notably, the SOUSSA pitching moment is in the fourth quandrant of the complex plane for all three Mach numbers.

To summarize briefly, in general the three different analyses and the experiment give lift and pitching-moment results which agree among themselves at least fairly well, except for the unsteady experimental moment on the clean wing at $M = 0.8$ and the unsteady Dusto-calculated moment on the wing plus tip body at $M = 0.8$. SOUSSA, with its zero-order panel approximation (i.e., uniform velocity potential on each panel), has performed rather

well in comparison with experimental results and with PANAIR, a higher order panel method.

Concluding Remarks

Application of a generalized Green's function method to the velocity-potential differential equation transforms it into an integral-differential delay equation which can be implemented for computation by surface panelling. The prototype surface-panel computer program SOUSSA P1.1, which is based on this concept, calculates subsonic steady and unsteady pressure distributions and integrated forces on bodies of arbitrary shape and deformation.

In an earlier validation and critique of the SOUSSA panel method, calculations were made for six simple configurations. The purpose of the present report was to extend the validation to a geometrically more complex and more realistic configuration, that of an instrumented F-5 wing model with and without a tip-mounted missile.

Calculated lift and moment results were compared with experimental results. Steady and unsteady results were obtained at Mach numbers M of 0.6, 0.8, and 0.9 at steady pitch angles of 0° and ±0.5° and for small pitching oscillations at 20 and 40 Hz. For the clean wing, where variations of the SOUSSA panelling were used, very good convergence was indicated at $M = 0.6$ for steady flow, but for unsteady pitching oscillations the modest differences at 40 Hz indicated less assured convergence with respect to panelling. For the wing with tip body, panelling variations were not performed.

The agreement of SOUSSA calculations with experimental results ranged from very good to fairly good with the exception of the unsteady pitching-moment slope on the clean wing at $M = 0.8$, for which the experiment may conceivably be in error. The SOUSSA results also agreed reasonably well with most of the results from three different PANAIR and PANAIR-related programs. A steady-flow-only PANAIR program produced distinctly poorer agreement for lift and pitching moment for uniform chordwise panelling (i.e., with a "large" leading-edge panel) than for a modified cosine panelling distribution (with a much smaller leading-edge panel).

In general the SOUSSA program, the experiments, and the three PANAIR-related programs gave lift and pitching-moment results which agreed at least fairly well, except for the unsteady clean-wing experimental moment at $M = 0.8$ and a moment calculated with a PANAIR predecessor at $M = 0.8$ on the wing with tip body. SOUSSA, with its zero-order panel approximation (i.e., uniform velocity potential on each panel), has performed rather well compared with experiment and with a higher-order panel method, PANAIR.

NASA Langley Research Center
Hampton, VA 23665-5225
June 12, 1987

References

Cunningham, Herbert J.; Desmarais, Robert N.; and Yates, E. Carson, Jr. 1982: *Steady, Oscillatory, and Unsteady Subsonic and Supersonic Aerodynamics—Production Version 1.1 (SOUSSA—P1.1). Volume II—User/ Programmer Manual, Addendum 1—Analytical Treatment of Wake Influence.* NASA TM-84484.

Derbyshire, Thomas; and Sidwell, Kenneth W. 1982: *PAN AIR Summary Document (Version 1.0).* NASA CR-3250.

Dusto, A. R. 1980: *Aerodynamic Analysis of a Fighter Aircraft With a Higher Order Paneling Method.* AFWAL-TR-80-3115, U.S. Air Force, Nov. (Available from DTIC as AD A099 404.)

Dusto, Arthur R.; and Epton, Michael A. 1980: *An Advanced Panel Method for Analysis of Arbitrary Configurations in Unsteady Subsonic Flow.* NASA CR-152323.

Magnus, Alfred E.; and Epton, Michael A. 1980: *PAN AIR—A Computer Program for Predicting Subsonic or Supersonic Linear Potential Flows About Arbitrary Configurations Using a Higher Order Panel Method. Volume I—Theory Document (Version 1.0).* NASA CR-3251.

Morino, Luigi 1974: *A General Theory of Unsteady Compressible Potential Aerodynamics.* NASA CR-2464.

Morino, Luigi 1980: *Steady, Oscillatory, and Unsteady Subsonic and Supersonic Aerodynamics—Production Version (SOUSSA-P 1.1). Volume I—Theoretical Manual.* NASA CR-159130.

Smolka, Scott A.; Preuss, Robert D.; Tseng, Kadin; and Morino, Luigi 1980: *Steady, Oscillatory, and Unsteady Subsonic and Supersonic Aerodynamics—Production Version 1.1 (SOUSSA-P 1.1). Volume II—User/ Programmer Manual.* NASA CR-159131.

Tijdeman, H.; Van Nunen, J. W. G.; Kraan, A. N.; Persoon, A. J.; Poestkoke, R.; Roos, R.; Schippers, P.; and Siebert, C. M. 1978: *Transonic Wind Tunnel Tests on an Oscillating Wing With External Stores. Part I—General Description.* AFFDL-TR-78-194, Pt. I, U.S. Air Force, Dec.

Tijdeman, H.; Van Nunen, J. W. G.; Kraan, A. N.; Persoon, A. J.; Poestkoke, R.; Roos, R.; Schippers, P.; and Siebert, C. M. 1979: *Transonic Wind Tunnel Tests on an Oscillating Wing With External Stores. Part II—The Clean Wing.* AFFDL-TR-78-194, Pt. II, U.S. Air Force, Mar.

Tijdeman, H.; Van Nunen, J. W. G.; Kraan, A. N.; Persoon, A. J.; Poestkoke, R.; Roos, R.; Schippers, P.; and Siebert, C. M. 1979: *Transonic Wind Tunnel Tests on*

an Oscillating Wing With External Stores. Part III—The Wing With Tip Store. AFFDL-TR-78-194, Pt. III, U.S. Air Force, May.

Yates, E. Carson, Jr.; Cunningham, Herbert J.; Desmarais, Robert N.; Silva, Walter A.; and Drobenko, Bohdan 1982: *Subsonic Aerodynamic and Flutter Characteristics of Several Wings Calculated by the SOUSSA P1.1 Panel Method.* NASA TM-84485.

Yates, E. Carson, Jr. 1986: Problems and Progress in Aeroelasticity for Interdisciplinary Design. Paper presented at the Symposium on Recent Trends in Aeroelasticity, Structures, and Structural Dynamics (Gainesville, Florida), Feb. 6–7.

Table I. Results for Clean Wing

(a) $M = 0.6$, steady (fig. 4(a))

Source	α, deg	C_Z	C_{L_α}	C_M	C_{M_α}
Experiment, run 136	−0.5	−0.0342		−0.0116	
Experiment, run 137	0	−.0093	3.06	−.0096	0.241
Experiment, run 138	.5	.0192		−.0074	
SOUSSA, 10 × 10,	−0.5	−0.0367		−0.0116	
uniform	0	−.0050	3.632	−.0088	0.323
	.5	.0267		−.0060	
SOUSSA, 12 × 12,	−0.5	−0.0376		−0.0113	
uniform	0	−.0059	3.627	−.0085	0.320
	.5	.0257		−.0057	
SOUSSA, 13 × 13,	−0.5	−0.0348		−0.0112	
cosine, modified	0	−.0031	3.621	−.0084	0.324
	.5	.0285		−.0055	
Dusto (1980, table 8)	−0.5	−0.0318		−0.00935	
	0	.0010	3.762	−.00721	0.245
	.5	.0338		−.00508	
PANAIR(S),	−0.5	−0.0119		−0.0164	
10 × 10, uniform	0	.0198	3.64	−.0145	0.218
	.5	.0516		−.0126	
PANAIR(S), 13 × 13,	−0.5	−0.0343		−0.0106	
cosine, modified	0	−.0024	3.66	−.0087	0.227
	.5	.0296		−.0067	

(b) $M = 0.8$, steady (fig. 4(b))

Source	α, deg	C_Z	C_{L_α}	C_M	C_{M_α}
Experiment, run 145	−0.5	−0.0318		−0.0125	
Experiment, run 146	0	−.0082	3.09	−.0117	0.195
Experiment, run 147	.5	.0222		−.0091	
SOUSSA, 13 × 13,	−0.5	−0.0390		−0.0136	
uniform	0	−.0040	4.013	−.0105	0.360
	.5	.0311		−.0073	
Dusto (1980)	−0.5	−0.0346		−0.0109	
	0	.0014	4.13	−.0087	0.260
	.5	.0375		−.0064	
PANAIR(U), 13 × 13,	−0.5	−0.0403		−0.0175	
cosine, modified	0	−.0063	3.88	−.0142	0.390
	.5	.0275		−.0107	

Table I. Concluded

(c) $M = 0.6$, unsteady (fig. 5(a))

Source	Frequency, Hz	C_{L_α}	C_{M_α}
Experiment	0	$3.060 + 0.0i$	$0.241 + 0.0i$
Experiment, run 382	20	$3.097 + 0.702i$	$.280 - 0.195i$
Experiment, run 383	40	$3.075 + 1.621i$	$.294 - 0.372i$
SOUSSA, 10×10,	0	$3.632 + 0.0i$	$0.323 + 0.0i$
uniform	40	$3.514 + 1.275i$	$.352 - 0.449i$
SOUSSA, 13×13,	0	$3.621 + 0.0i$	$0.324 + 0.0i$
cosine, modified	20	$3.568 + 0.680i$	$.327 - 0.253i$
	40	$3.540 + 1.457i$	$.353 - 0.502i$
Dusto (1980), 13×13,	0	$3.76 + 0.0i$	$0.245 + 0.0i$
cosine, modified	40	$3.78 + 1.084i$	$.354 + 0.464i$
PANAIR(S),13×13,	0	$3.661 + 0.0i$	$0.227 + 0.0i$
cosine, modified			

(d) $M = 0.8$, unsteady (fig. 5(b))

Source	Frequency, Hz	C_{L_α}	C_{M_α}
Experiment	0	$3.090 + 0.0i$	$0.195 + 0.0i$
Experiment, run 367	20	$2.938 + 0.609i$	$-.039 - 0.141i$
Experiment, run 368	40	$3.132 + 1.281i$	$-.027 - 0.323i$
SOUSSA, 13×13,	0	$4.013 + 0.0i$	$0.360 + 0.0i$
uniform	20	$3.994 + 0.428i$	$.355 - 0.281i$
	40	$4.044 + 0.922i$	$.347 - 0.569i$
Dusto (1980), 13×13,	0	$4.130 + 0.0i$	$0.260 + 0.0i$
cosine, modified	40	$4.483 + 0.531i$	$.335 - 0.577i$
PANAIR(U), 13×13,	0	$3.88 + 0.0i$	$0.390 + 0.0i$
cosine, modified	20	$3.85 + 0.34i$	$.447 - 0.275i$
	40	$3.85 + 0.726i$	$.425 - 0.527i$

Table II. Wing With Tip Body

(a) $M = 0.6$, steady (fig. 6(a))

Source	α, deg	C_Z	C_{L_α}	C_Z^*	$C_{L_\alpha}^*$	C_M	C_{M_α}	C_M^*	$C_{M_\alpha}^*$
Experiment, run 255	−0.5	−0.0471		−0.00113		−0.0120		−0.00075	
Experiment, run 256	0	−.0086	3.97	−.00002	0.128	−.0101	0.241	−.00018	0.0493
Experiment, run 257	.5	.0221		.00110		−.0078		.00039	
SOUSSA, 10 × 10,	−0.5	−0.0403		−0.00119		−0.0113		−0.00075	
uniform	0	−.0056	3.98	−.00020	0.128	−.0088	0.298	−.00018	0.0493
	.5	.0292		.00080		−.0062		.00039	

(b) $M = 0.9$, steady (fig. 6(b))

Source	α, deg	C_Z	C_{L_α}	C_Z^*	$C_{L_\alpha}^*$	C_M	C_{M_α}	C_M^*	$C_{M_\alpha}^*$
Experiment, run 249	−0.5	−0.0528		−0.00149		−0.0171		−0.00071	
Experiment, run 251	0	−.0091	4.73	−.00008	0.164	−.0138	0.286	−.00020	0.058
Experiment, run 252	.5	.0297		.00137		−.0121		.00030	
SOUSSA, 10 × 10,	−0.5	−0.0469		−0.00144		−0.0154		−0.00092	
uniform	0	−.0042	4.89	−.00017	0.145	−.0124	0.344	−.00023	0.0779
	.5	.0384		.00109		−.0094		.00044	

(c) $M = 0.6$, unsteady (fig. 7(a))

Source	Frequency, Hz	C_{L_α}	$C_{Z_\alpha}^*$	C_{M_α}	$C_{M_\alpha}^*$
Experiment	0	$3.97 + 0.0i$	$0.128 + 0.0i$	$0.241 + 0.0i$	$0.0493 + 0.0i$
Experiment, run 258	20	$3.31 + 0.810i$	$.131 + 0.0245i$	$.212 - 0.198i$	$.0474 + 0.0019i$
SOUSSA, 10 × 10,	0	$3.977 + 0.0i$	$0.114 + 0.0i$	$0.298 + 0.0i$	$0.065 + 0.0i$
uniform	20	$3.893 + 0.592i$	$.112 + 0.028i$	$.301 - 0.245i$	$.064 - 0.00135i$
	40	$3.824 + 1.321i$	$.109 + 0.059i$	$.328 - 0.484i$	$.063 - 0.00039i$

(d) $M = 0.8$, unsteady (fig. 7(b))

Source	Frequency, Hz	C_{L_α}	$C_{Z_\alpha}^*$	C_{M_α}	$C_{M_\alpha}^*$
SOUSSA, 10 × 10,	0	$4.483 + 0.0i$	$0.130 + 0.0i$	$0.323 + 0.0i$	$0.0428 + 0.0i$
uniform	40	$4.439 + 0.924i$	$.129 + 0.042i$	$.305 - 0.595i$	$.0408 - 0.0175i$
Dusto (1980), 13 × 13,	0	$4.595 + 0.0i$	$0.203 + 0.0i$	$0.339 + 0.0i$	$0.0447 + 0.0i$
cosine, modified	40	$4.421 + 0.656i$	$.165 + 0.0270i$	$-.247 - 0.640i$	$.0549 - 0.0083i$

(e) $M = 0.9$, unsteady (fig. 7(c))

Source	Frequency, Hz	C_{L_α}	$C_{Z_\alpha}^*$	C_{M_α}	$C_{M_\alpha}^*$
Experiment	0	$4.73 + 0.0i$	$0.164 + 0.0i$	$0.286 + 0.0i$	$0.0579 + 0.0i$
Experiment, run 253	20	$4.13 + 0.138i$	$.170 + 0.0060i$	$.231 - 0.381i$	$.0550 + 0.0075i$
SOUSSA, 10 × 10,	0	$4.89 + 0.0i$	$0.144 + 0.0i$	$0.344 + 0.0i$	$0.0456 + 0.0i$
uniform	20	$4.91 + 0.397i$	$.145 + 0.0184i$	$.306 - 0.449i$	$.0442 - 0.0130i$

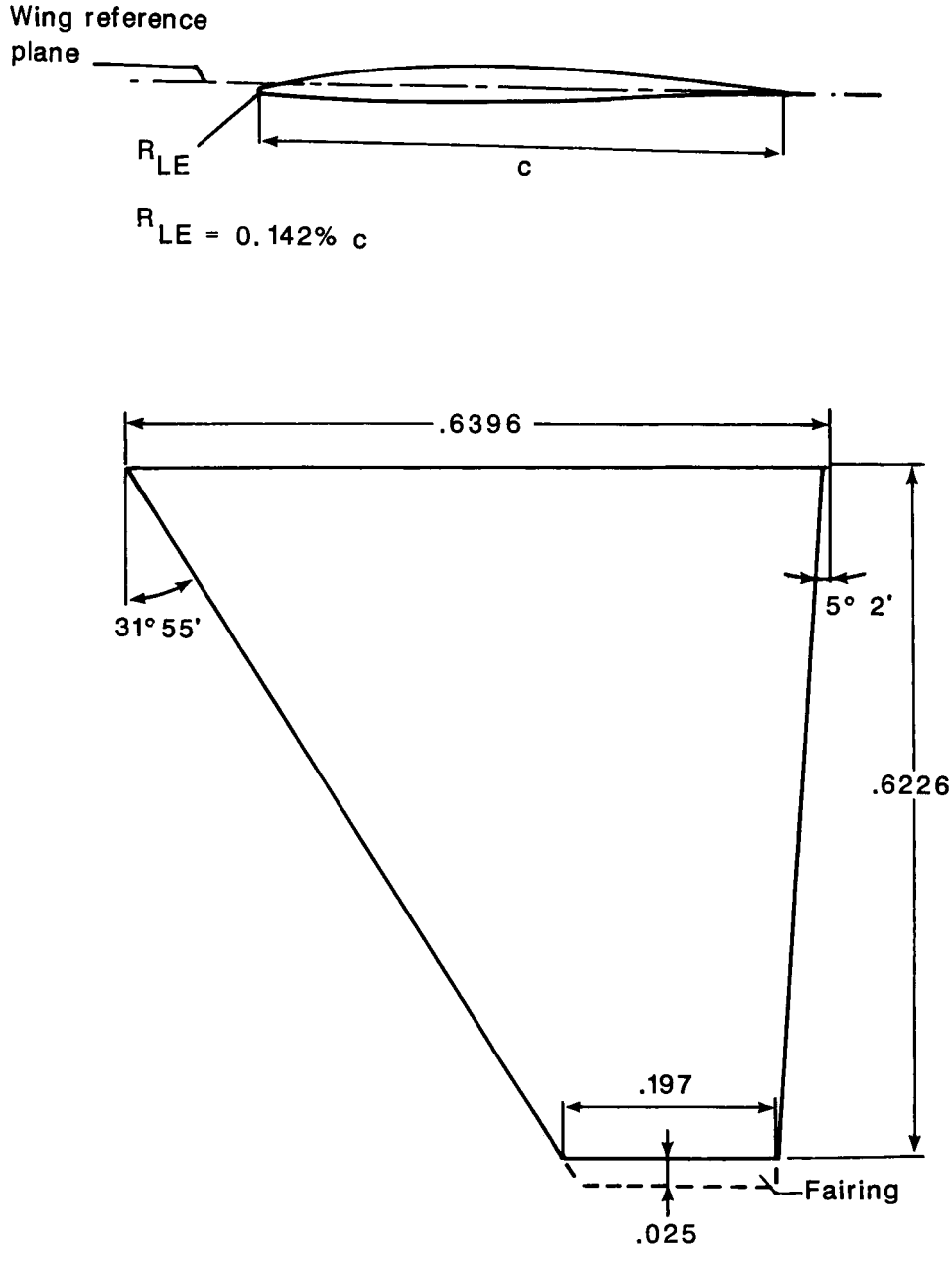

Figure 1. Clean wing with tip fairing indicated. Linear dimensions are in meters.

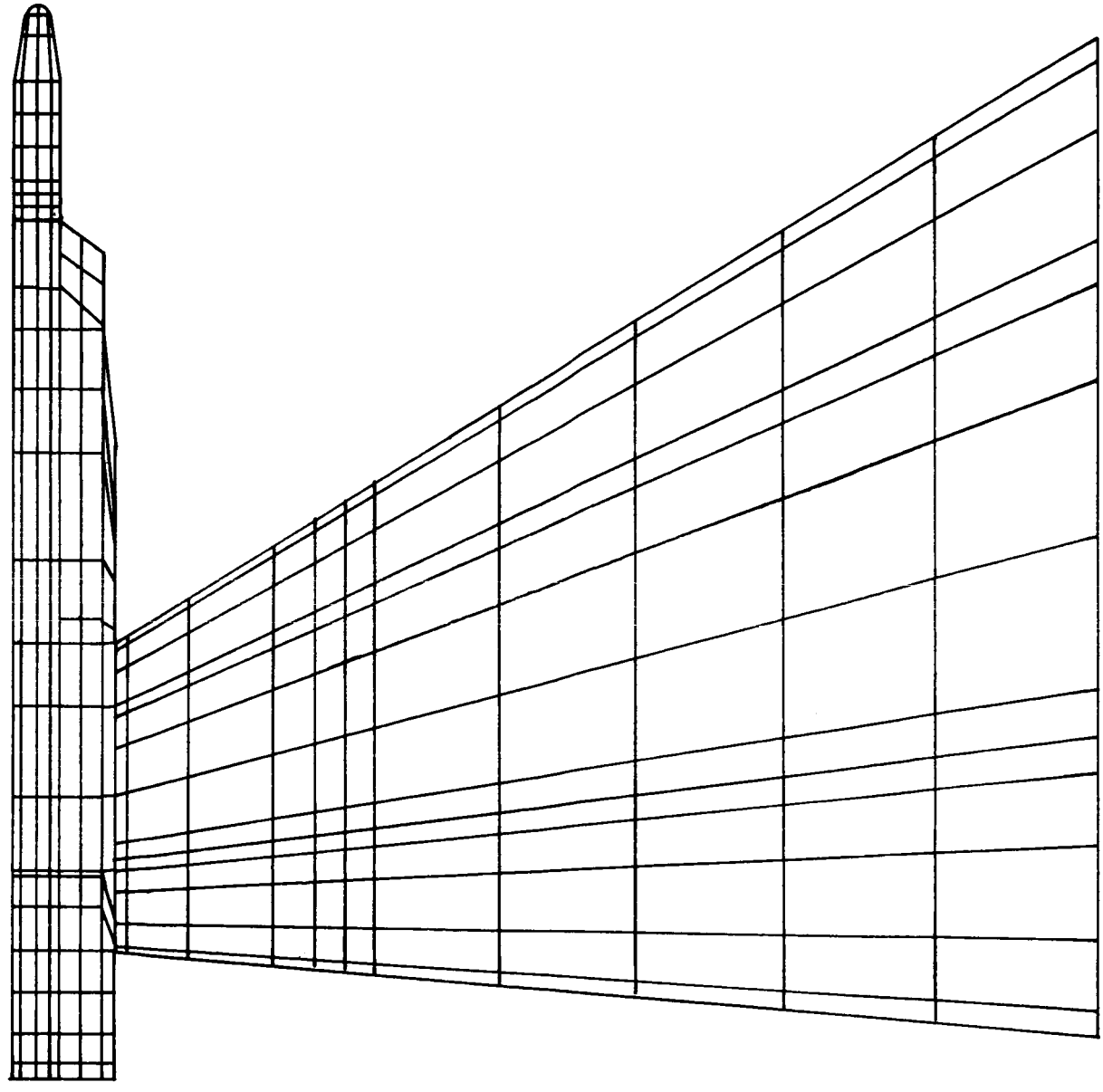

Figure 2. Wing with launcher and missile body, showing Dusto (1980) panelling.

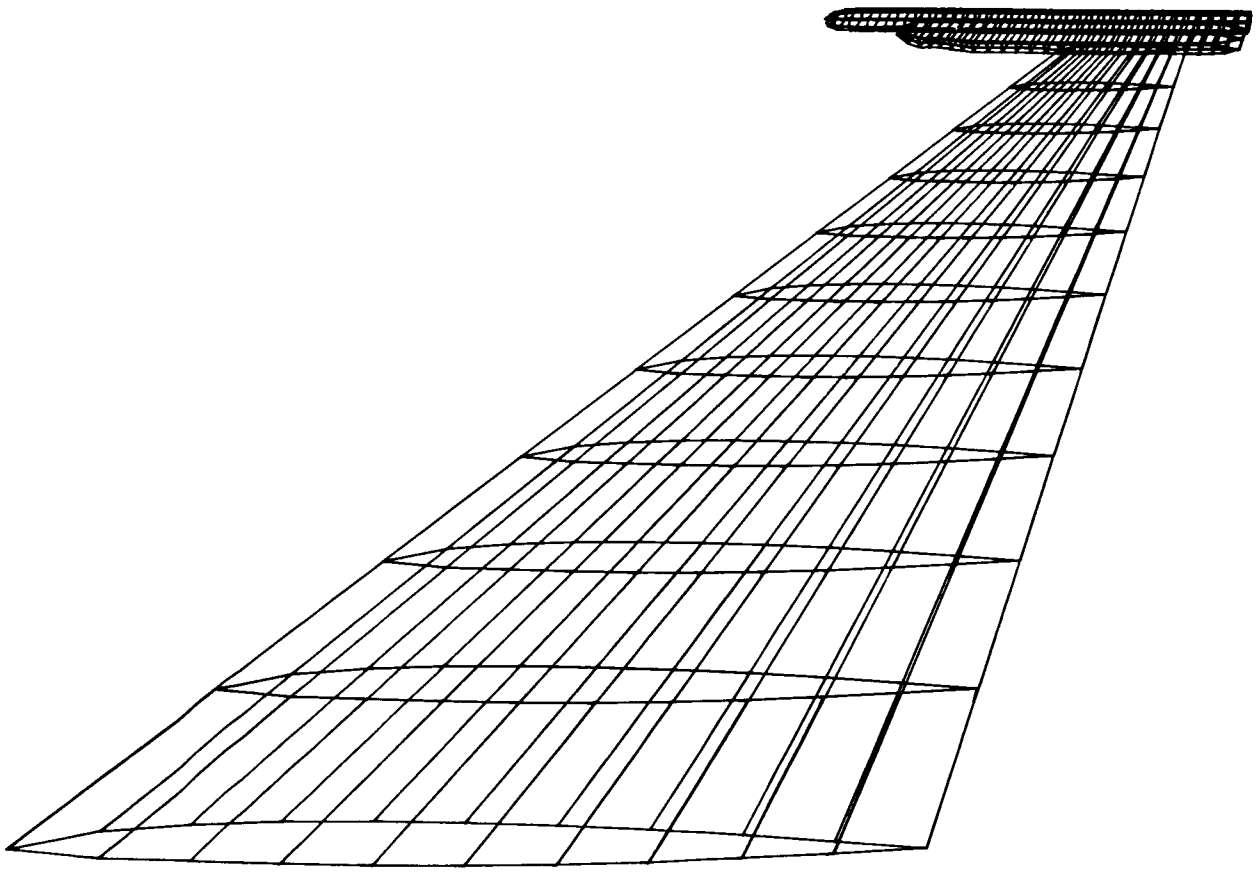

(a) Wing with tip body.

Figure 3. SOUSSA 10×10 uniform wing panelling (total of 634 panels).

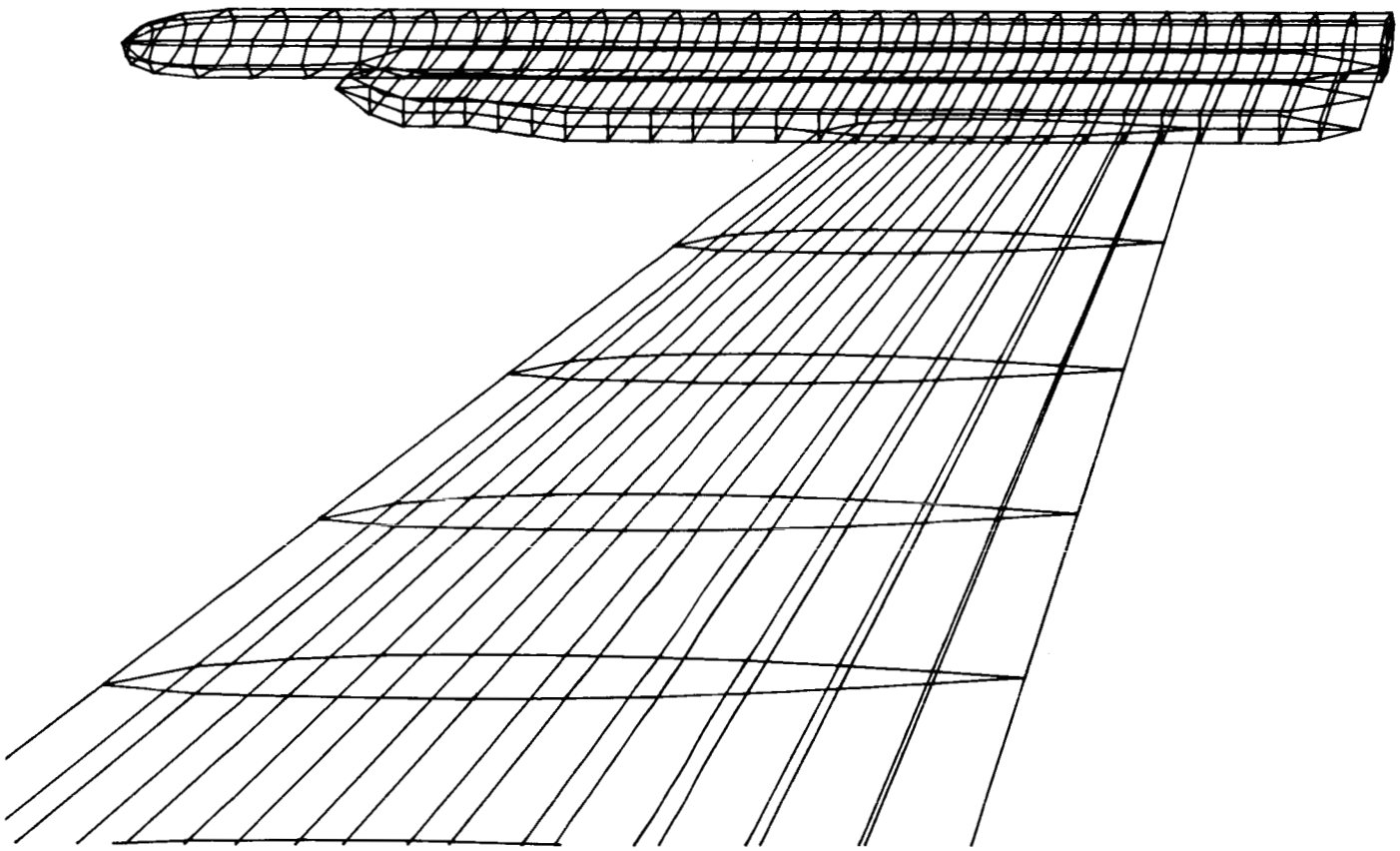

(b) Close-up of tip body.

Figure 3. Concluded.

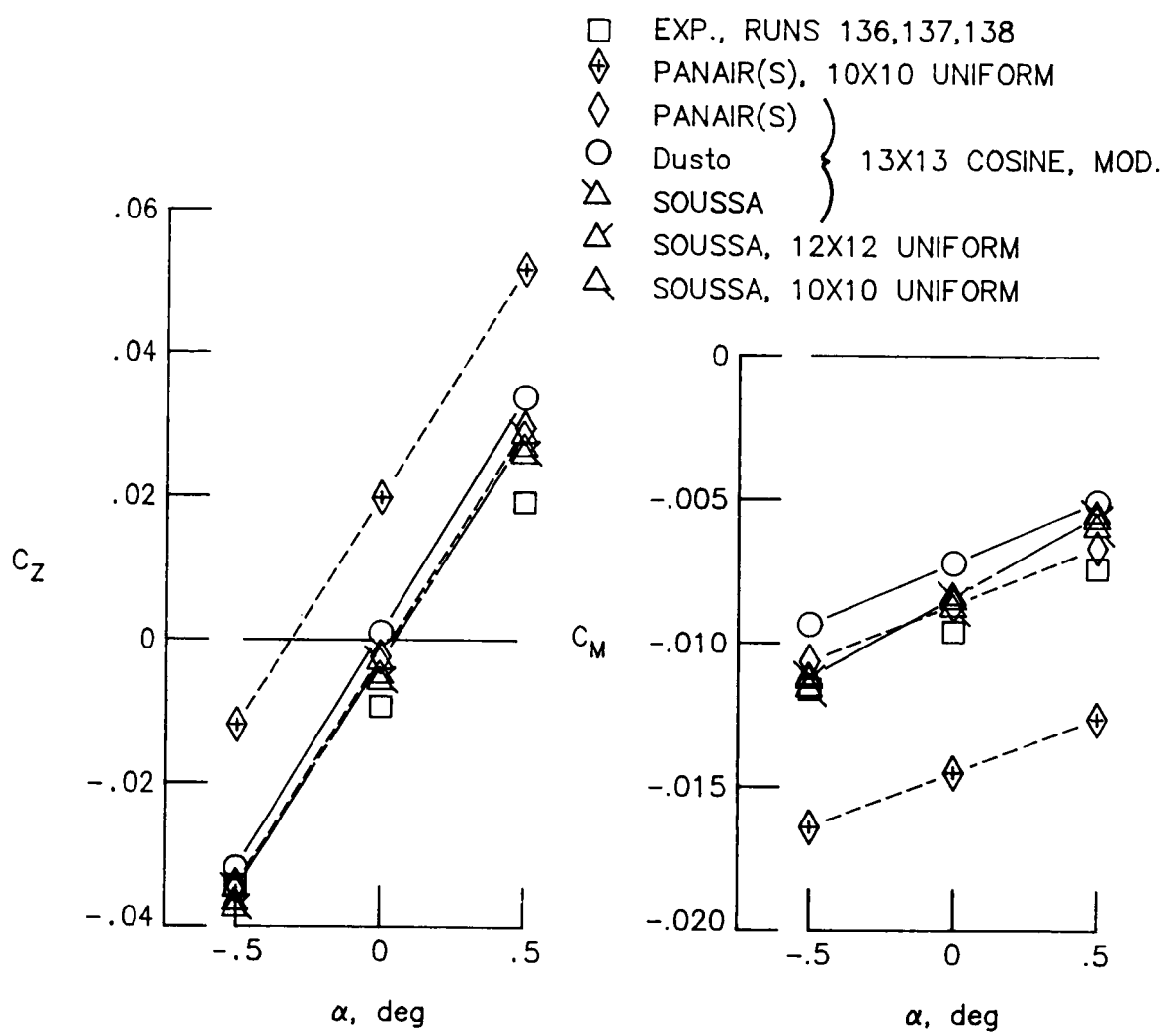

(a) $M = 0.6$, lift and moment.

Figure 4. Steady lift, pitching-moment, and pressure coefficients for clean wing.

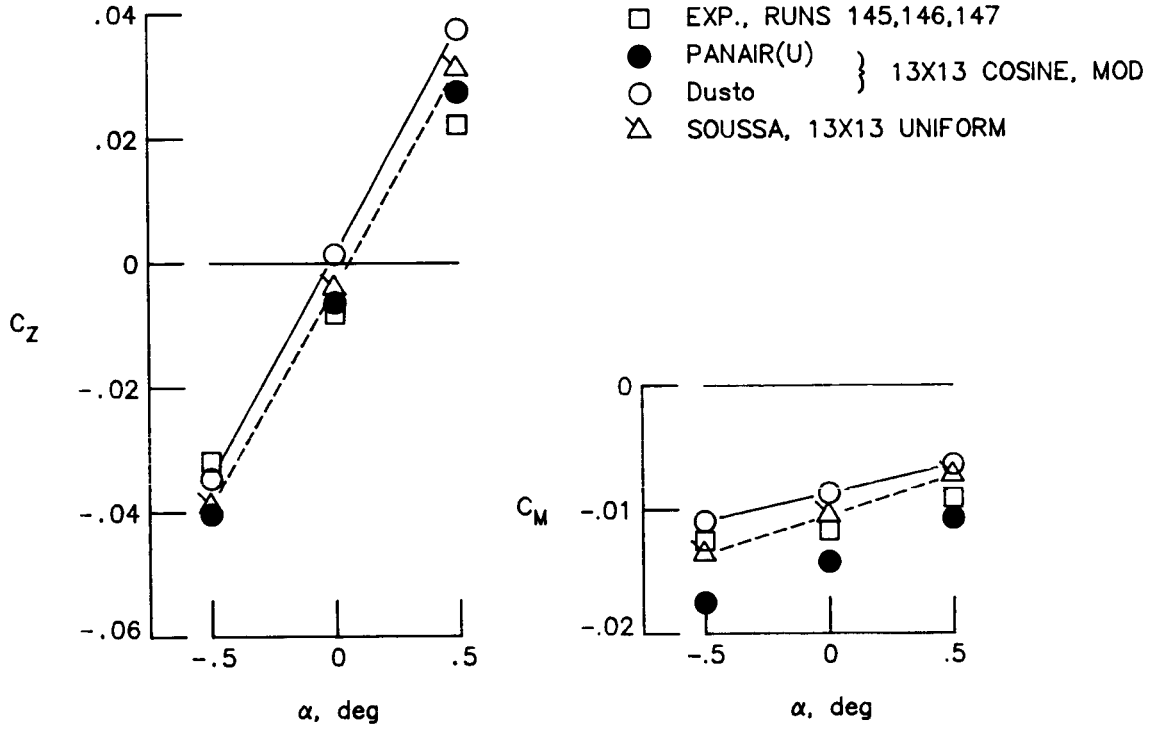

(b) $M = 0.8$, lift and moment.

Figure 4. Continued.

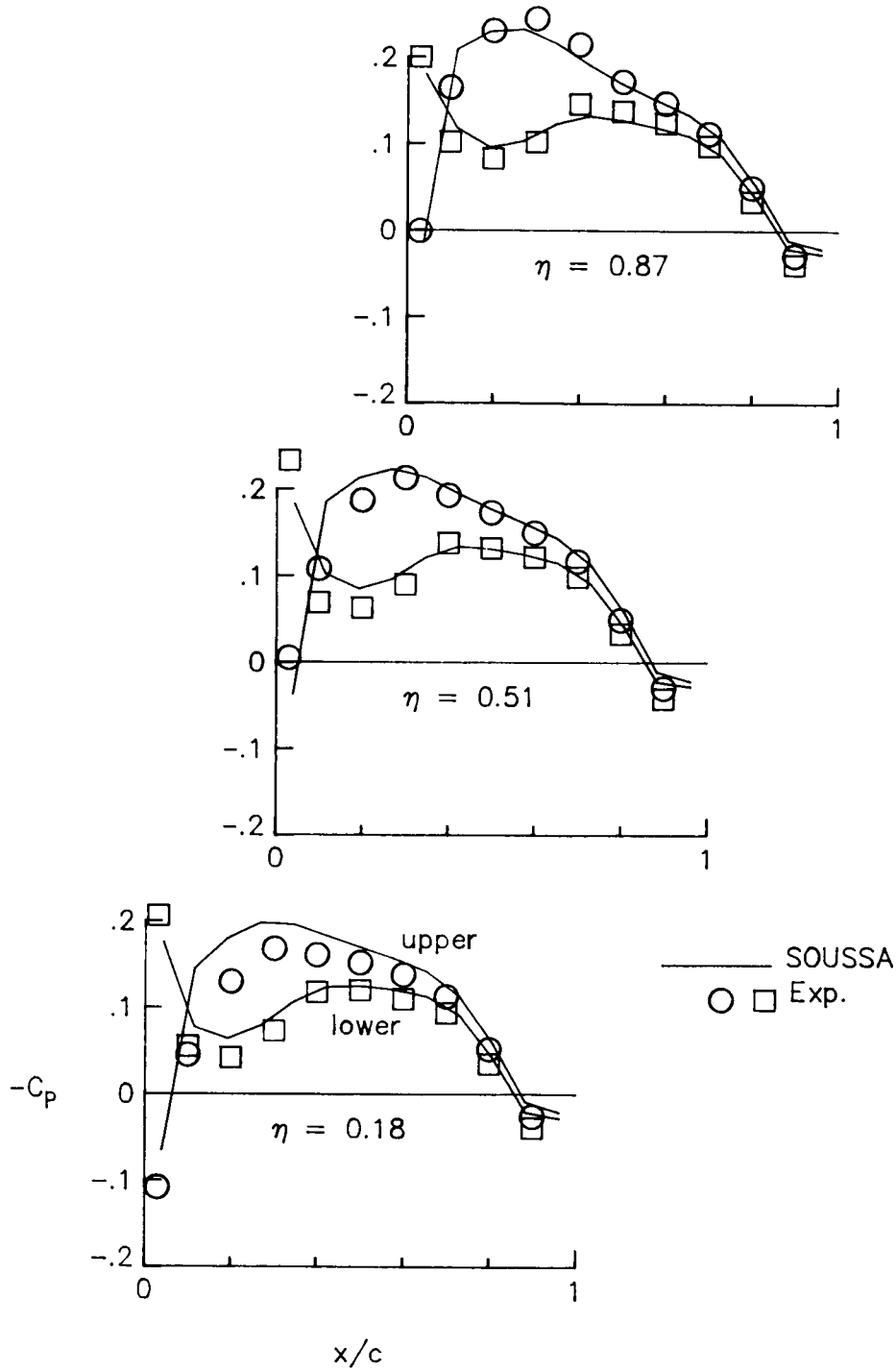

(c) $M = 0.8$, upper- and lower-surface pressures at three span stations for $\alpha = 0.5°$.

Figure 4. Concluded.

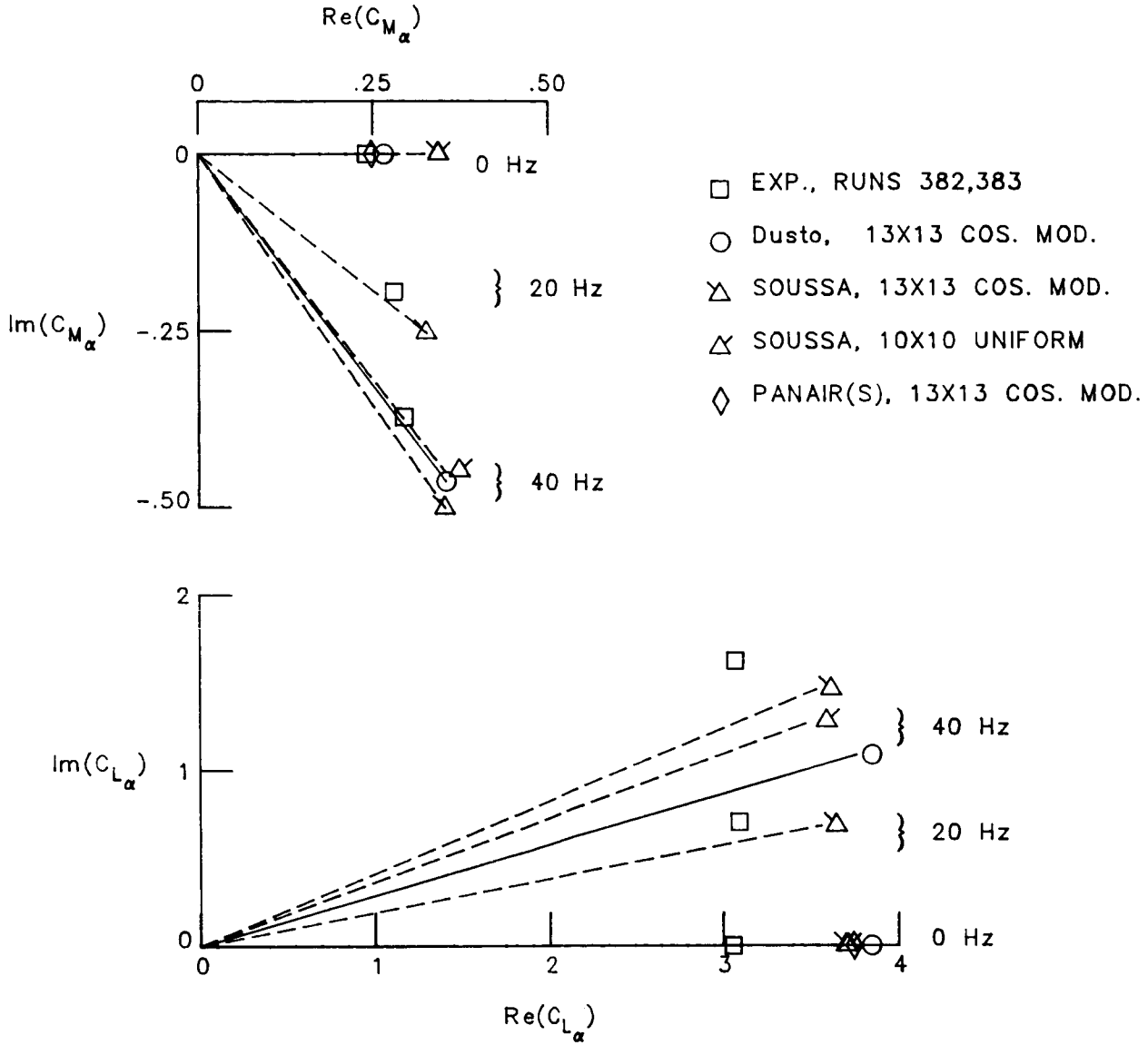

(a) $M = 0.6$, lift and pitching-moment slopes.

Figure 5. Unsteady lift, pitching-moment, and pressure slopes for clean wing pitching about $\alpha = 0°$.

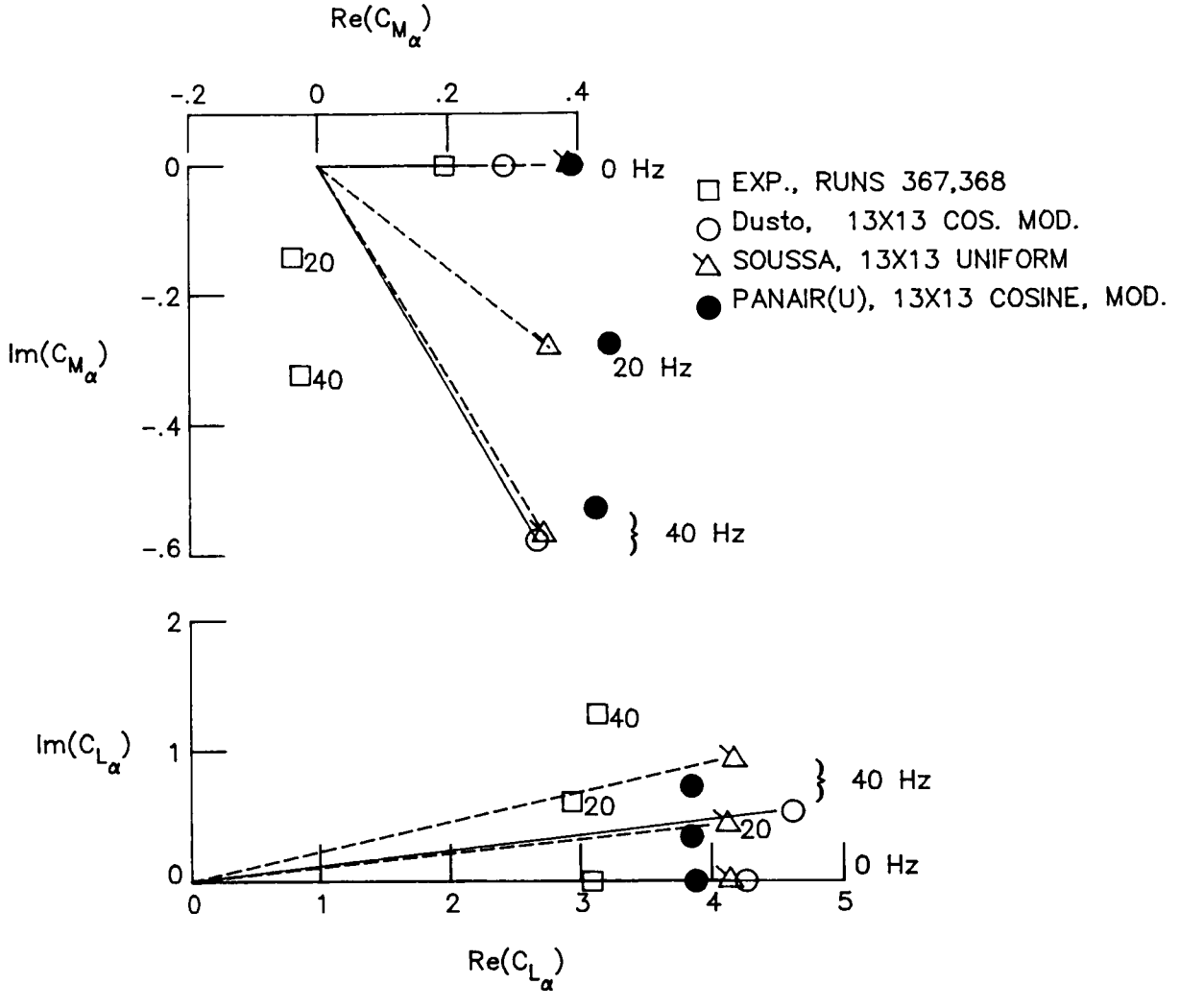

(b) $M = 0.8$, lift and pitching-moment slopes.

Figure 5. Continued.

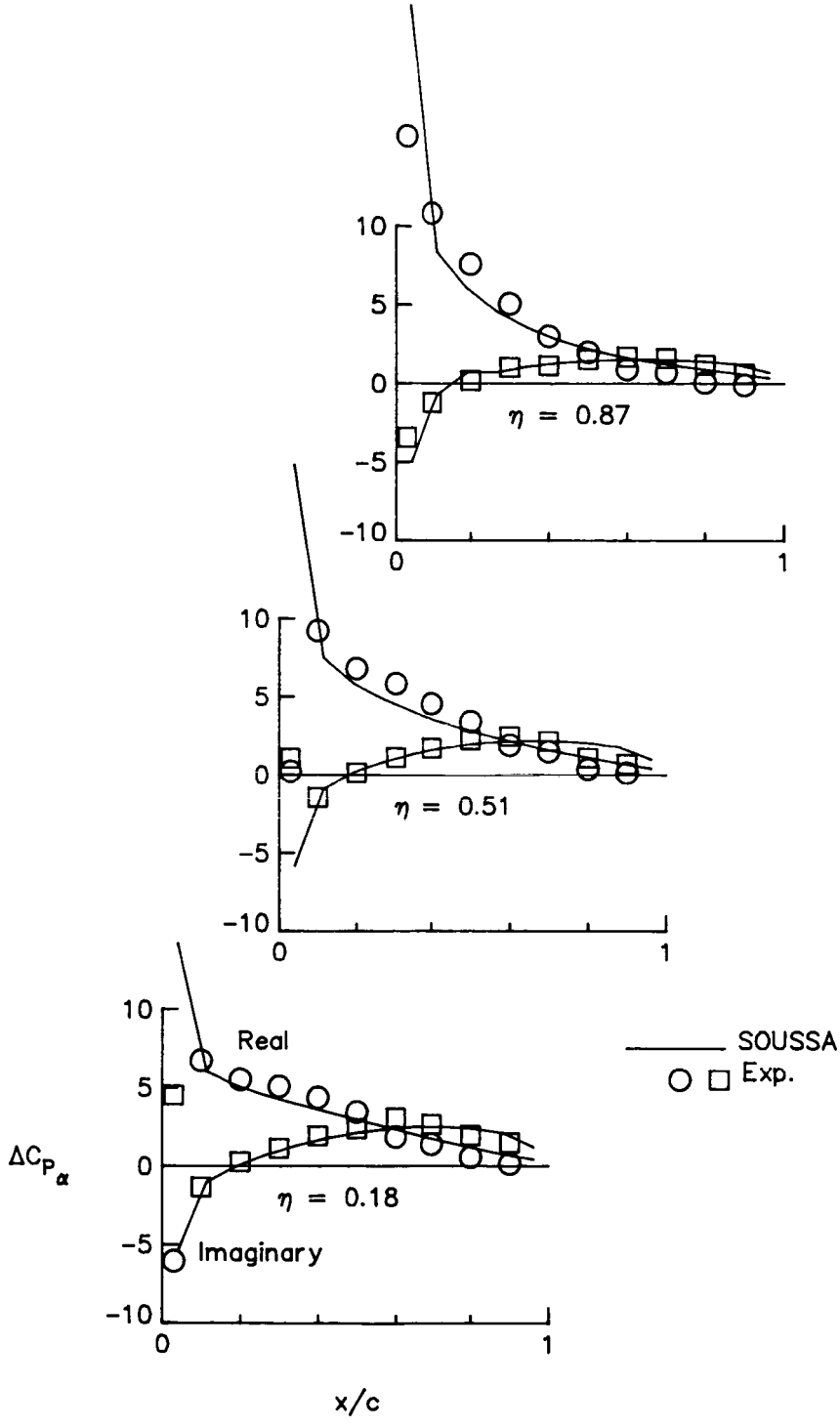

(c) $M = 0.8$, real and imaginary lifting-pressure slopes at three span stations for 40 Hz.

Figure 5. Concluded.

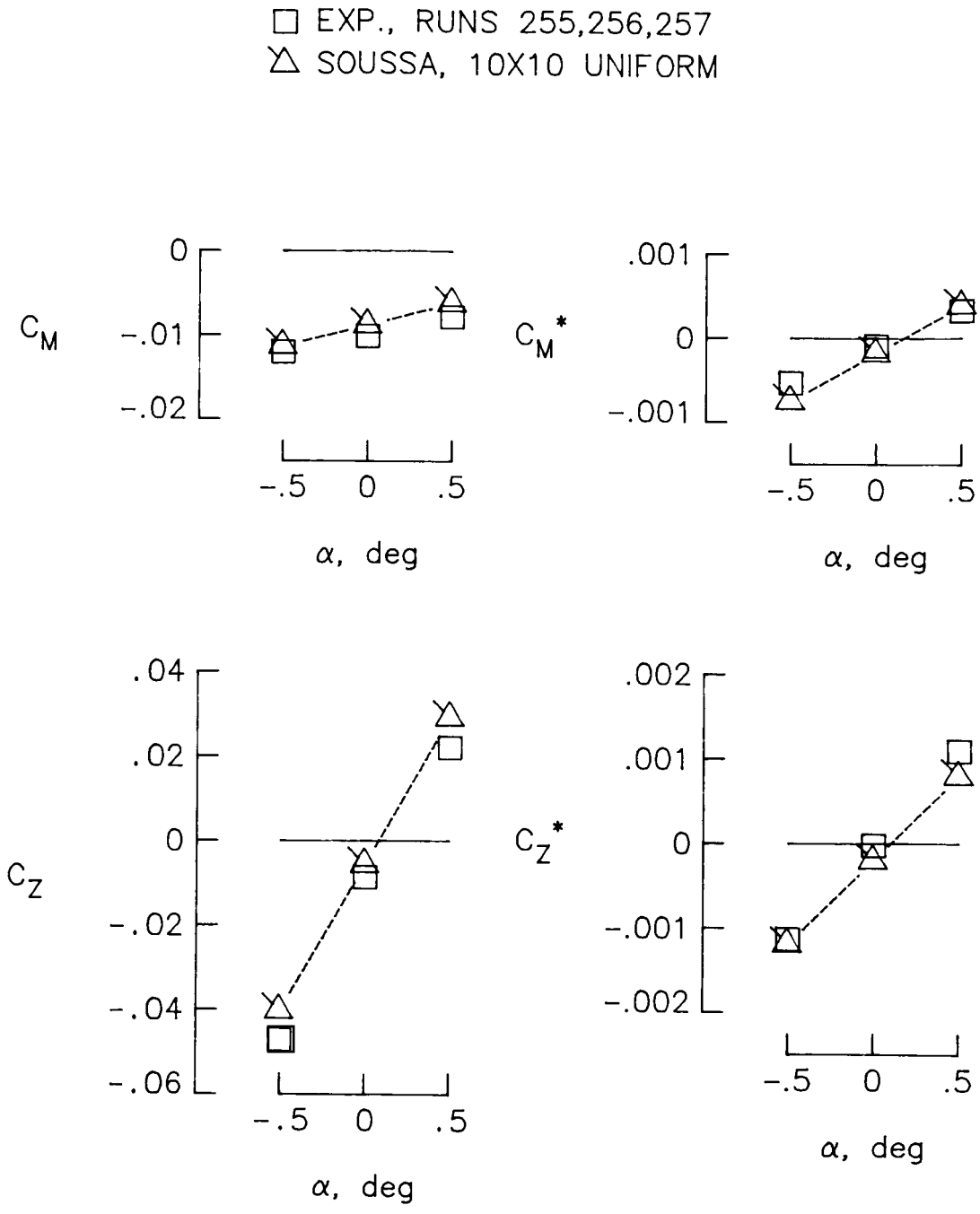

(a) $M = 0.6$.

Figure 6. Steady lift and pitching-moment coefficients on wing with tip body and contributions from tip body itself.

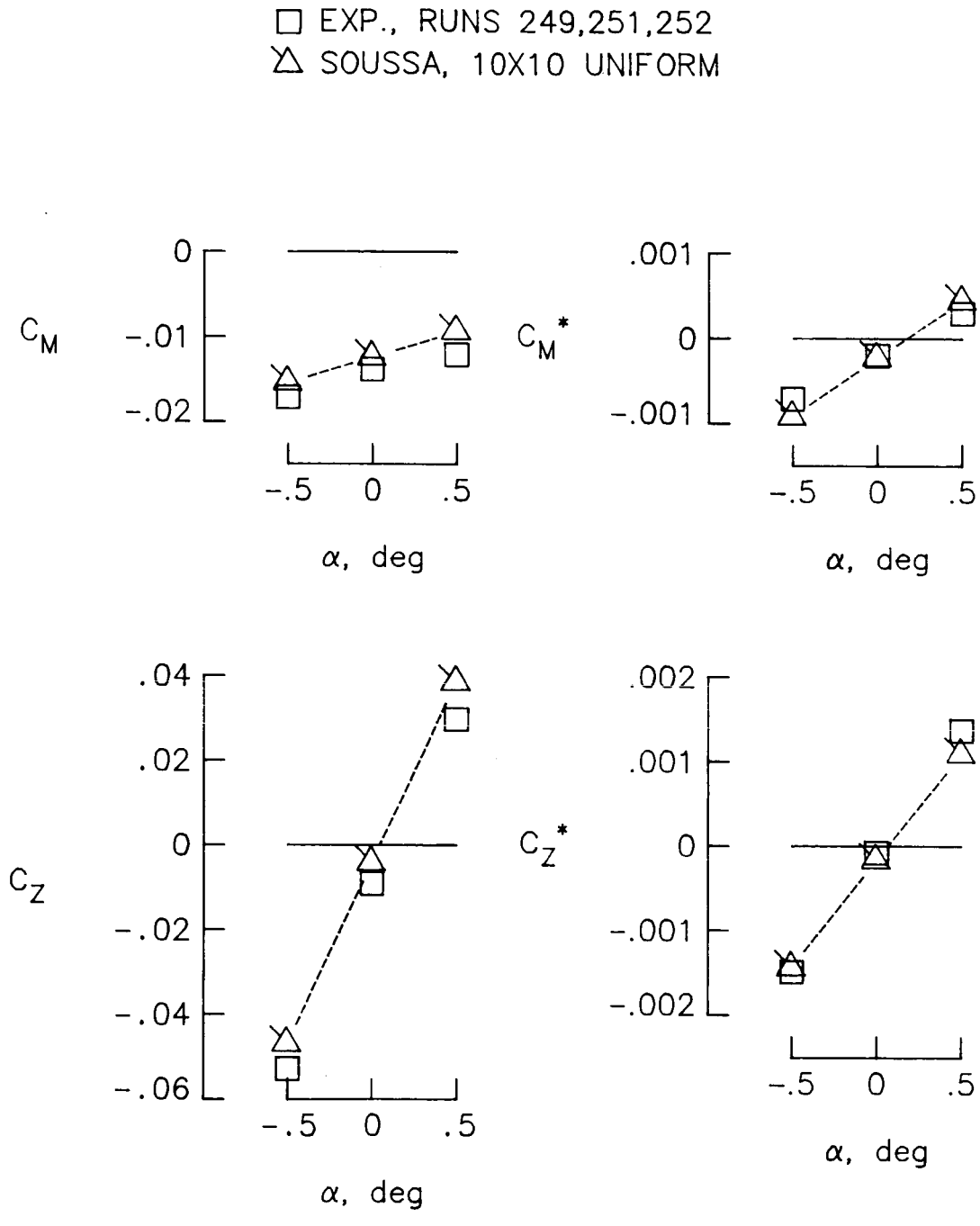

(b) $M = 0.9$.

Figure 6. Concluded.

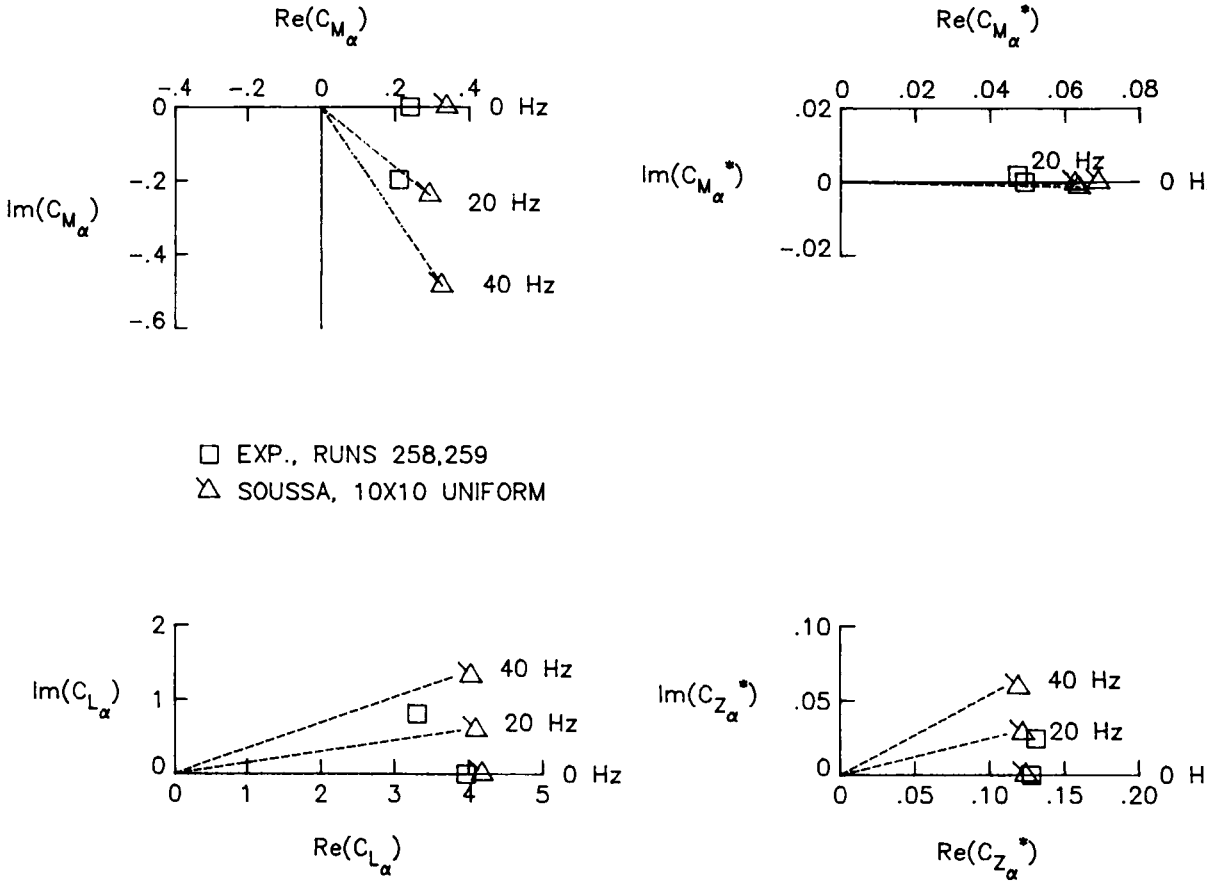

(a) $M = 0.6$.

Figure 7. Unsteady lift and pitching-moment coefficients on wing with tip body and contributions from tip body itself.

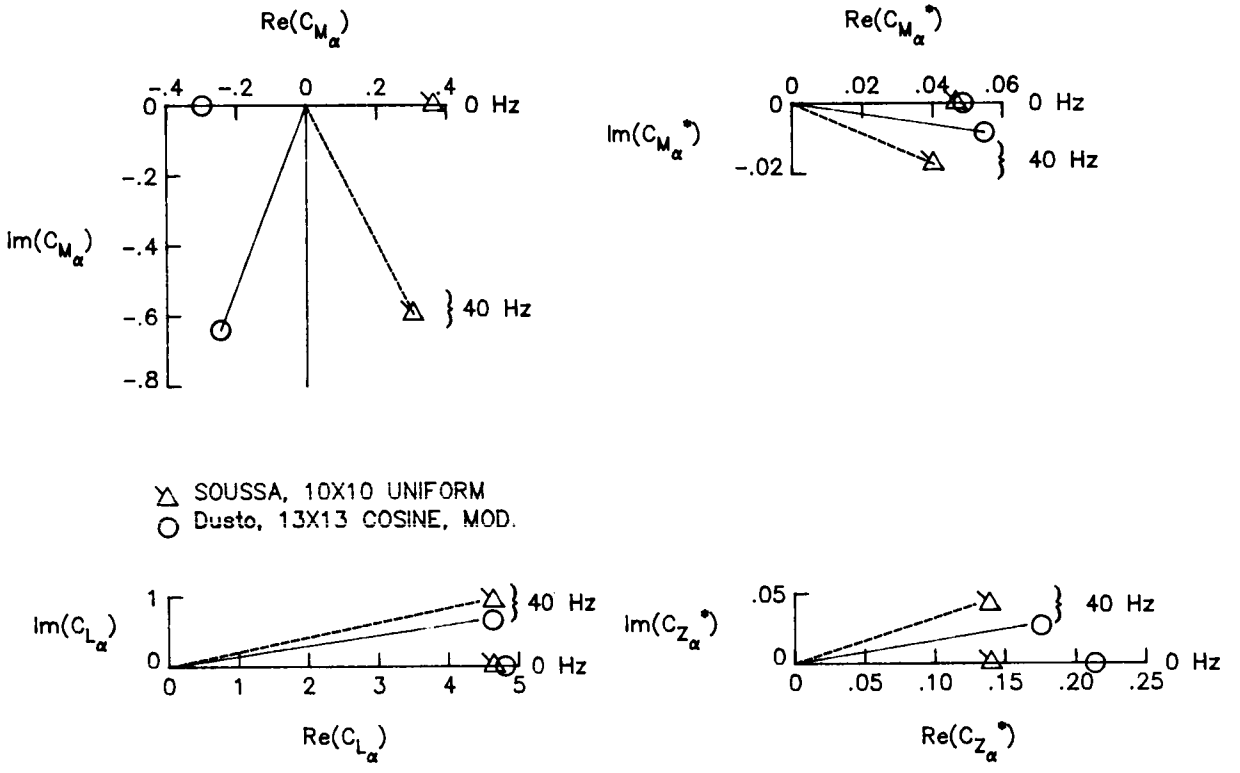

(b) $M = 0.8$.

Figure 7. Continued.

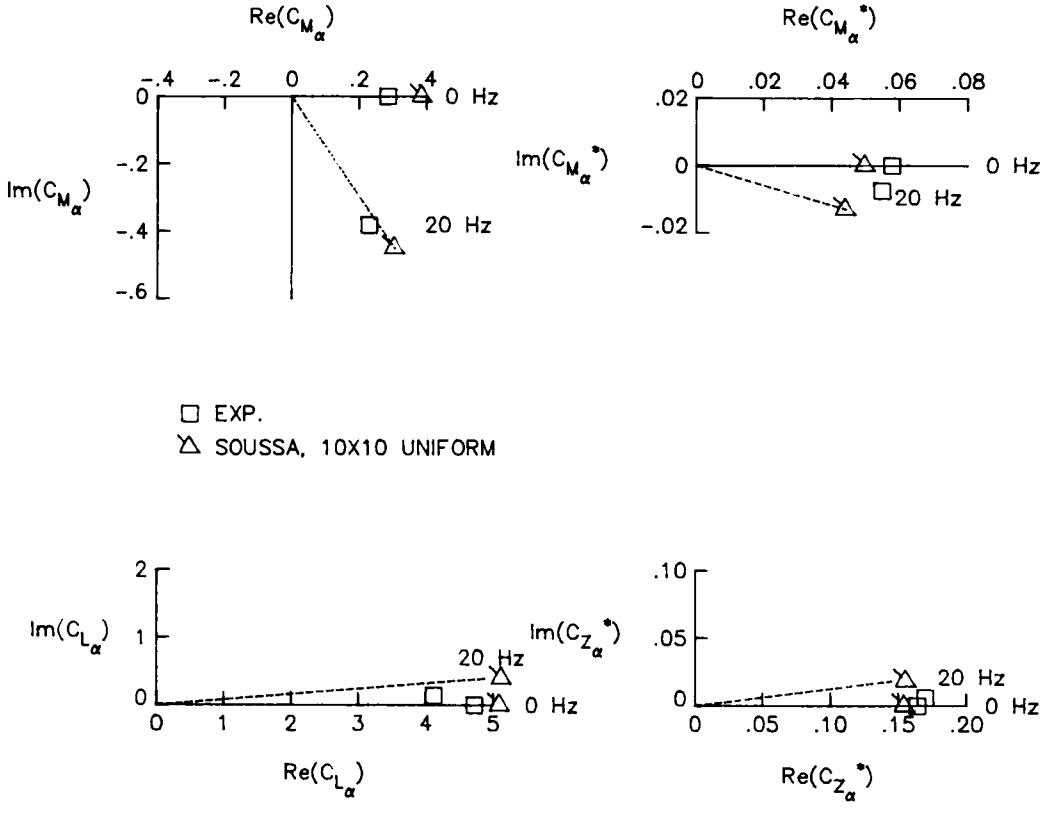

(c) $M = 0.9$.

Figure 7. Concluded.

NASA
National Aeronautics and Space Administration

Report Documentation Page

1. Report No.	2. Government Accession No.	3. Recipient's Catalog No.
NASA TP-2736		

4. Title and Subtitle	5. Report Date
Steady and Unsteady Aerodynamic Forces From the SOUSSA Surface-Panel Method for a Fighter Wing With Tip Missile and Comparison With Experiment and PANAIR	August 1987
	6. Performing Organization Code
7. Author(s)	8. Performing Organization Report No.
Herbert J. Cunningham	L-16262
9. Performing Organization Name and Address	10. Work Unit No.
NASA Langley Research Center Hampton, VA 23665-5225	505-63-21-01
	11. Contract or Grant No.
12. Sponsoring Agency Name and Address	13. Type of Report and Period Covered
National Aeronautics and Space Administration Washington, DC 20546-0001	Technical Paper
	14. Sponsoring Agency Code

15. Supplementary Notes

16. Abstract

The body surface-panel method SOUSSA is applied to calculate steady and unsteady lift and pitching-moment coefficients on a thin fighter-type wing model with and without a tip-mounted missile. Comparisons are presented with experimental results and with PANAIR and PANAIR-related calculations for Mach numbers from 0.6 to 0.9. In general the SOUSSA program, the experiments, and the PANAIR (and related) programs give lift and pitching-moment results which agree at least fairly well, except for the unsteady clean-wing experimental moment and the unsteady moment on the wing with tip body calculated by a PANAIR-predecessor program at a Mach number of 0.8.

17. Key Words (Suggested by Authors(s))

Aerodynamic forces
Panel methods
Aeroelasticity
Flutter
Unsteady flow
Green's function

18. Distribution Statement

Unclassified—Unlimited

Subject Category 02

19. Security Classif.(of this report)	20. Security Classif.(of this page)	21. No. of Pages	22. Price
Unclassified	Unclassified	27	A03

NASA FORM 1626 OCT 86

NASA-Langley, 1987

For sale by the National Technical Information Service, Springfield, Virginia 22161-2171